Angle-resolved two-dimensional mapping of electron emission from the inner-shell $2p$ excitations in Cl_2

O. Nayandin,[1] E. Kukk,[1,*] A. A. Wills,[1,†] B. Langer,[2] J. D. Bozek,[3] S. Canton-Rogan,[1] M. Wiedenhoeft,[1] D. Cubaynes,[4] and N. Berrah[1]

[1]*Physics Department, Western Michigan University, Kalamazoo, Michigan 49008*

[2]*Max-Born-Institut, Max-Born-Strasse 2A, 12489 Berlin, Germany*

[3]*Lawrence Berkeley National Laboratory, University of California, Berkeley, California 94720*

[4]*Laboratoire de Spectrosopie Atomique et Ionique, Université Paris–Sud, Orsay, France*

(Received 9 November 2000; published 16 May 2001)

Angle-resolved Auger and valence photoelectron spectra were measured over a 14-eV photon energy range across the Cl_2 $2p$ ionization thresholds. The measurements were carried out using highly efficient time-of-flight spectrometers coupled with photons from the Atomic and Molecular undulator beamline of the Advanced Light Source and an advanced data-acquisition system. Auger-electron spectra of $2p \rightarrow \sigma^*$ and $2p \rightarrow nl$ resonances were analyzed and the evolution of the resonant Auger to the normal Auger decay distorted by postcollision interaction was examined. We find that valence photoionization channels do not resonate strongly at the photon energies of the core-to-Rydberg excitation, in contrast to the strongly resonating ones observed in the HCl molecule. Auger decay spectra of the $2p^{-1}\sigma^*$ resonances showed no evidence of atomic transitions in Cl*, also in contrast to HCl. In addition, angular distribution of the photoelectron and Auger-electron lines was derived.

DOI: 10.1103/PhysRevA.63.062719 PACS number(s): 33.80.Eh, 32.80.Hd, 33.60.Cv

I. INTRODUCTION

Inner-shell processes in small molecules have been studied with growing interest during recent years. Constantly improving experimental techniques have revealed new details in Auger-electron and photoelectron spectra, such as anisotropy of electron emission [1–10], molecular field splitting [11], and postcollision interaction [7,12]. Studies of the resonant Auger processes in hydrogen halide molecules such as HBr [13], HCl, and DCl [7,9,14,15] showed that the excitation to the lowest unoccupied antibonding σ^* orbital is followed by two competing processes: molecular dissociation and Auger decay. The branching ratio of ''molecular'' versus ''atomic'' Auger transitions increases with increasing reduced mass [15,16]. It was also shown in HCl that the dissociation rate was changing with the photon energy [7,9]. However, only a few experimental studies of these phenomena were done in the heavier homonuclear molecule Cl_2 and only at a few selected photon energies [15–17].

In this work, we present a complete angle-resolved two-dimensional (2D) experimental image of the electron emission from Cl_2 following photoexcitation and photoionization of Cl $2p$ core levels. It was measured using electron time-of-flight (TOF) spectrometers coupled with photons from the Advanced Light Source (ALS). To generate a continuous 2D electron emission pattern, we scanned the photon energy with 20- and 100-meV steps over a 14-eV-wide energy range collecting electron kinetic-energy spectra for each energy at two angles simultaneously. This technique is angle-resolved, and fully differential, therefore the electron angular distribution as well as the relative partial cross sections of the spectral structures were obtained at different resonant and nonresonant excitation energies.

II. EXPERIMENT

The experiment was performed in a two-bunch operation on the high-resolution Atomic, Molecular and Optical Physics undulator beam line (10.0.1) at the ALS at Lawrence Berkeley National Laboratory. Details of the experimental setup used to perform two-dimensional angle-resolved photoelectron spectroscopic studies are given elsewhere [18,19], hence only a brief description will be given here. The electron-energy spectra (EES) were measured using two time-of-flight (TOF) analyzers mounted on a rotatable vacuum chamber, perpendicular to the axis of the synchrotron radiation beam with one analyzer positioned at $\theta = 0°$ and the other at $\theta = 54.7°$ (magic angle) with respect to the electric-field vector. Chlorine gas was introduced into the interaction region through a 0.5-mm inner diameter needle, maintaining a pressure of about 2×10^{-5} Torr in the chamber. This configuration allowed us to accumulate EES simultaneously at two angles. As a result, angular anisotropies can be measured and the β parameters can be extracted for the individual final ionic states. The EES were collected for 15 s, then the photon energy was incremented by 20 meV to generate two-dimensional (photon and electron energy) spectra (2D EES) at two angles.

A 163-V retarding voltage was used to disperse the flight times of the energetic electrons and thus improve the energy resolution, estimated as 1% of the kinetic energy of the electrons. Calibration spectra of Ne $2s$ and $2p$ photoelectron lines were used to obtain the scaling factors for the time-to-energy conversion and to generate the electron transmission efficiency of the analyzers as a function of kinetic energy

*Present address: Department of Physics, Oulu University, Oulu FIN-90570, Finland.

†Present address: Fritz-Haber-Institut der Max-Planck-Gesellschaft, Faradayweg 4-6, 14195 Berlin, Germany.

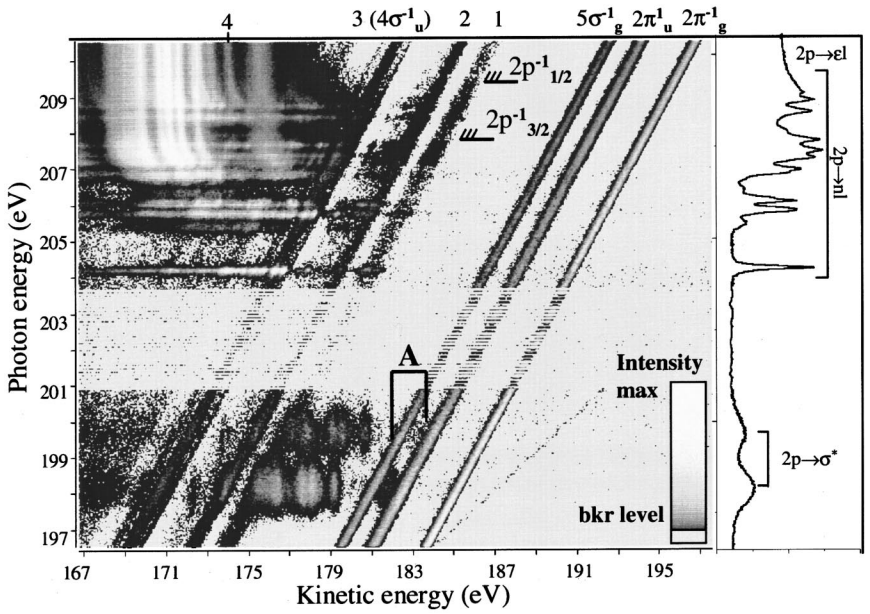

FIG. 1. Two-dimensional (2D) map of electron emission from the Cl_2 molecule across the Cl $2p$ ionization threshold, taken at 54.7 relative to the polarization vector. Photon-energy step is 20 meV, and 100 meV for the region from 201 to 203.6 eV. The summed electron yield is shown on the right.

[20]. All spectra in the 2D EES data sets have been converted from time to energy scale, and corrected for transmission efficiency, variation in photon flux, and collection time. The photon-energy resolution was set to 75 meV for this experiment. The resulting 2D spectra illustrate the evolution of the electron-emission process as the photon energy is scanned toward and across the Cl $2p$ ionization thresholds, as shown in Fig. 1. To extract individual Auger and constant ionic state spectra as well as total electron yields, we used our custom-made 2D data analysis software based on previous development [19]. In addition to the comprehensive 2D EES, several individual photoelectron spectra were collected for 1000 s at the photon energies corresponding to ''on'' and ''off'' resonance for the transitions $2p_{3/2,1/2} \rightarrow \sigma^*$ (antibonding transitions) and $2p_{3/2} \rightarrow 4s,4p$ (Rydberg transitions). Resonance positions were determined from the total electron yield as a function of photon energy extracted from the 2D EES.

III. RESULTS AND DISCUSSION

A. 2D map of the electron emission and total electron yield

A 2D map of the photoelectron emission pattern of Cl_2 measured at 54.7° with respect to the polarization vector of the incident radiation is shown in the main panel of Fig. 1. The intensity of the electron signal is represented in different shades of gray. Electrons emitted with the same kinetic energy at different photon energies are aligned vertically in the 2D map and those emitted with constant binding energy from diagonal lines.

The electron yield, summed over the kinetic-energy range of the 2D map, is shown in the right-hand panel of Fig. 1 as a function of photon energy. The spectrum contains two groups of resonance features due to excitation to the σ^* antibonding orbital and to Rydberg series of molecular orbitals ($2p \rightarrow nl$). That is in contrast to the spectrum of atomic chlorine, which does not have a well-behaved Rydberg series. This was demonstrated by the detailed photoelectron study of Caldwell *et al.* [21], where a rich structure with no Rydberg demarcation was observed. The measured width of the $2p_{3/2} \rightarrow \sigma^*$ and $2p_{1/2} \rightarrow \sigma^*$ resonances in Cl_2 is 980(20) meV, obtained from the fit of two Gaussian profiles. Sharp peaks in the photon-energy region of 203–209 eV are a combination of Rydberg resonance structures with widths ranging from 103 meV for the $2p_{3/2} \rightarrow 4s$ excitation to 362 meV for lines corresponding to the $2p_{3/2} \rightarrow 4p$ excitation.

The electron emission *patterns* in the 2D map reflect the different characters of the three regions in the absorption spectrum. The excitations to the antibonding σ^* orbital ($2p \rightarrow \sigma^*$) can lead to the dissociation of the molecule, as observed in HCl [7,12,15], where the dissociation produces two atoms, one of which is core-excited. The dissociation competes with the Auger decay of the core-hole state and, depending on the relative time scale of these two processes, either molecular or atomic (or both) features can be observed in the Auger-electron spectrum. The Auger decay of these two resonances is represented on the 2D map in Fig. 1 as a series of vertical lines in the 172–184-eV kinetic-energy range, which is described in more detail in Sec. III C.

The excitation to the $2p \rightarrow ns,nd$ Rydberg orbitals leads to resonant Auger decays to the final ionic states that are represented in the 2D map as the horizontally aligned groups of higher-intensity peaks. The decay pattern gradually shifts towards the lower kinetic energy, starting at about 206-eV photon energy, and evolves into the normal Auger decay shown as vertical lines. This appears to be analogous to the trend seen in atoms [22] where the Rydberg electron undergoes changes in n during the transition to the final ionic state.

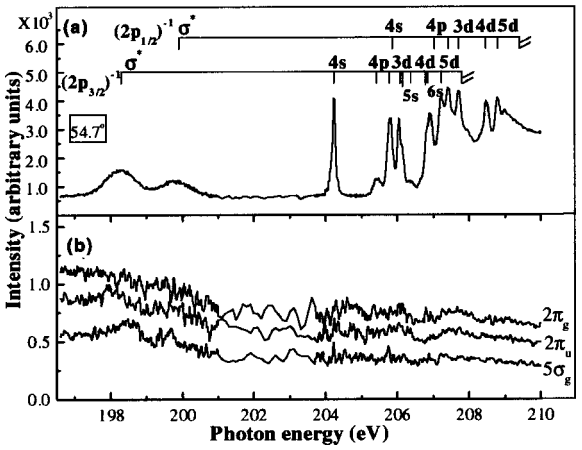

FIG. 2. (a) Summed electron yield of Cl_2 as a function of photon energy in the region of Cl $2p$ ionization threshold; resonance assignment is taken from Shaw *et al.* [17]; (b) partial electron yield of the $5\sigma_g$,$2\pi_u$,$2\pi_g$ photolines of Cl_2. Spectra extracted from the 2D map taken at 54.7° relative to the polarization vector.

This evolution is explained in the simple model by Ueda *et al.* [23] in the case of the Ca $3p$ excitation region.

Three strong diagonal lines on the right side of the 2D map represent valence photoionization (the $5\sigma_g$, $2\pi_u$, and $2\pi_g$ photoelectron lines). The 2D mapping technique also allows unambiguous identification of the three weaker diagonal lines, marked as 1, 2, and 3 in Fig. 1, as photoelectron lines with binding energies of 22.0, 23.7, and 27.1 eV, respectively. Line 3 at 27.1 eV has been identified as due to the $4\sigma_u$ photoionization [24], whereas assignment for peaks 1 and 2 is not available.

B. Photoelectron yields

The partial electron yields (or constant ionic state spectra) of the $5\sigma_g$, $2\pi_u$, and $2\pi_g$ photolines are plotted in panel (b) of Fig. 2, while the summed electron yield is plotted in panel (a). The partial electron yields have smoothly decreasing intensity across the measured photon-energy range. There is a small increase in the intensity of the $5\sigma_u$ and $2\pi_u$ lines in the photon-energy region 197–201 eV due to overlap with one of the final ionic states of the Auger decay of the $2p_{3/2}\rightarrow\sigma^*$ and $2p_{1/2}\rightarrow\sigma^*$ resonances. The transitions to this state are seen on the 2D map of Fig. 1 (marked by ''*A*'') as two vertical lines between the $5\sigma_g$ and $2\pi_u$ photon lines. From these measurements, we do not see any apparent enhancement of the $5\sigma_g$, $2\pi_u$, and $2\pi_g$ lines in the higher photon-energy region corresponding to the Cl $2p$ Rydberg resonances (203–209 eV), indicating, therefore, that the participator Auger decay channel (autoionization), which would lead to resonating photon lines, is negligible. Such a behavior is in contrast with the findings for HCl, where a strong participator decay channel was observed, particularly at the $2p_{3/2}^{-1}4s$ resonance [12].

C. Auger decay of molecular resonances

Auger decay following the $2p_{3/2}\rightarrow\sigma^*$, $2p_{1/2}\rightarrow\sigma^*$ excitations and normal Auger spectra at 220-eV photon energy, extracted from the 2D map, are shown in Fig. 3. One can observe resonant structures in Figs. 3(a) and 3(b), where known atomic chlorine lines would have been observed if dissociation had occurred [the line positions are marked in panel (a) of Fig. 3]. The dissociation process observed in HCl [7,12,15] produces hydrogen and core-excited chlorine atoms. In the case of HCl, the dissociation is fast enough that a large part of the Auger decay occurs in the atomic chlorine as the $2p^5 3p^6\rightarrow 3p^4$ transitions [7,12,15], giving rise to the familiar ^1S, ^1D, ^3P term structure of the np^{-2} final state. The width of these peaks reflects the lifetime broadening, further convoluted by the spectrometer resolution. The fraction of the Auger decay still occurring in the molecular environment adds pronounced tails and an enhanced irregular background to these lines. In Fig. 3, however, there is no clear evidence of such narrow atomic lines. We observe instead considerably broader peaks and a more complex general structure. There are, for example, two peaks in the region where the atomic chlorine ^1D line would appear. Moreover, the sum of the $2p_{3/2}\rightarrow\sigma^*$ and the $2p_{1/2}\rightarrow\sigma^*$ spectra, with photon lines removed, is similar to the normal molecular Auger spectra, taken at 220 eV [shown in panel (c) of Fig. 3]. In the case of normal Auger decay, the σ^* orbital remains unoccupied and the molecule will not disso-

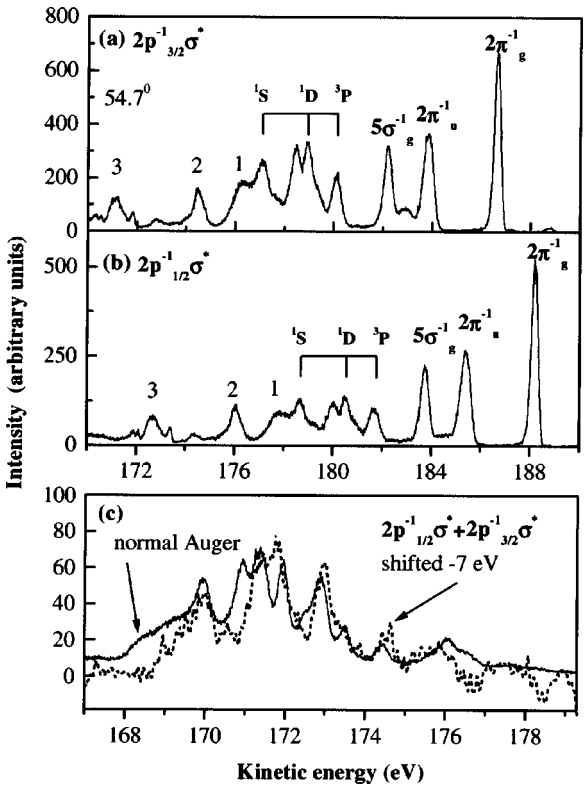

FIG. 3. Electron-energy spectra measured at 54.7° relative to polarization vector: (a) Auger decay of the $2p_{3/2}^{-1}$ σ^* resonance measured at 198.22 eV, (b) $2p_{1/2}^{-1}$ σ^* at 199.78 eV, (c) comparison of the sum of the $2p_{3/2}^{-1}$ σ^* and $2p_{1/2}^{-1}$ σ^* (dashed line, photolines removed, shifted by -7 eV in kinetic energy), with normal Auger decay at 220 eV (solid line). The labels $^1S, ^1D, ^3P$ show the positions of atomic lines if dissociation occurred; 1, 2, 3 show the positions of the inner valence photolines.

ciate. In the simplest picture, the molecular spectator Auger decay is like the normal Auger decay, creating similar final states with two holes in the valence orbitals of the molecule. The spectator electron is in a Rydberg orbital which has a screening effect that shifts the Auger spectrum towards higher kinetic energies. The lack of identifiable atomic features and the similarity of the resonant and nonresonant Auger spectra suggest that molecular spectator decay is the dominant process in the Cl_2 molecule.

According to the semiclassical view of the dissociation dynamics [13–15], the dissociation rate is determined by the reduced mass of the molecule and the shape of the potential-energy curve (PEC) of the dissociating state. The slope of the PEC's of the $2p^{-1}_{1/2,3/2}\sigma^*$ states can be determined from the width of the corresponding peak in the absorption (or total electron yield) spectrum. The observed width, 0.94 eV, of these resonances in Cl_2 is smaller by a factor of 1.9 than the width of the σ^* resonances in HCl [16]. The shape of such a resonance peak arises from the projection of the square of the $v=0$ ground-state vibrational wave function onto the excited state's antibonding PEC. If the slopes of the PEC's were equal for HCl and Cl_2, this projection would be about two times narrower for Cl_2 due to its larger reduced mass and narrow Franck-Condon region. The observed difference in the resonance widths could then be attributed to the effects of the different reduced mass, and one can assume that the shapes of the PEC's of the core-excited states are very similar for both molecules. The reduced mass also affects the dissociation rate. From numerical simulations of the Auger decay and dissociation in HCl [14], a tentative time limit $t_{\mathrm{HCl}}=5.8$ fs was established, after which the Auger decay becomes essentially atomic. In HCl, about 45% of the decay takes place after this limit [14]. If all other conditions are similar, this ''atomic limit'' is reached in Cl_2 after

$$t_{\mathrm{Cl}_2}=\left(\frac{\mu_{\mathrm{Cl}_2}}{\mu_{\mathrm{HCl}}}\right)^{1/2} t_{\mathrm{HCl}}, \tag{1}$$

where μ_{Cl_2} and μ_{HCl} are the reduced masses of the molecules. This gives $t_{\mathrm{Cl}_2}=24.6$ fs, and only about 3.5% of the decay takes place after that time period. Therefore, the much larger reduced mass of Cl_2 is sufficient to cause the lack of identifiable atomic features in the Auger spectrum of Cl_2.

Returning to Fig. 1, it is interesting to notice that the Auger-electron peaks at the $2p_{3/2}\rightarrow\sigma^*$ and the $2p_{1/2}\rightarrow\sigma^*$ resonances are at constant kinetic energy across the breadth of the resonance profiles. For atomic Auger lines, this would be expected, as the differences in the photon energy are absorbed by the nuclear motion in the dissociation process. The kinetic energy of molecular Auger lines, however, is predicted to depend on the photon energy nonlinearly near the absorption maximum and linearly (maintaining constant binding energy) at the far wings of the absorption band [25]. A closer examination of the photon-energy region from 197 to 201 eV in Fig. 1 gives no indication of dispersive behavior for the group of strong Auger lines at 175–181-eV kinetic energy, which seems to contradict the assignment of these lines as mainly of molecular origin. However, the region of

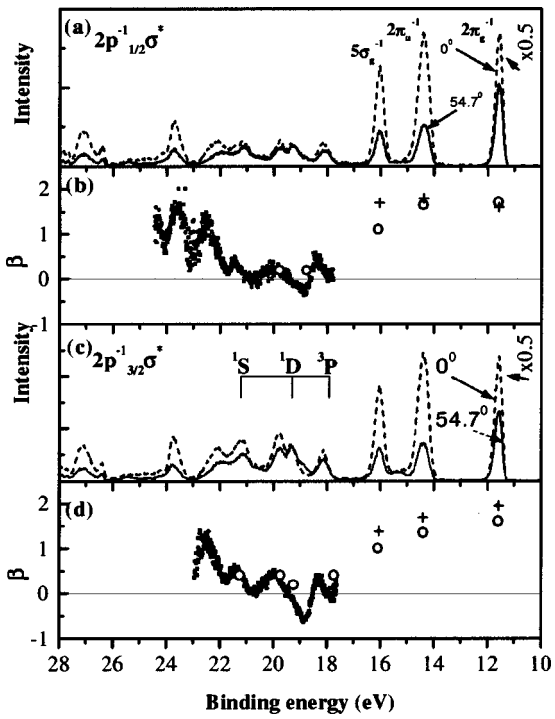

FIG. 4. Electron energy spectra, measured at the $2p\rightarrow\sigma^*$ resonances. (a), (c) Electron-energy spectra of $2p_{1/2}\rightarrow\sigma^*$,$2p_{3/2}\rightarrow\sigma^*$ resonances, taken at 0° and 54.7° relative to the polarization plane, respectively; intensity of the $2\pi_g^{-1}$ peak is divided by 2; (b), (d) the angular parameter β; open circles are the values from Ref. [16] and crosses are this work.

linear dispersion starts several half-widths at half maximum (HWHM) away from the resonance maximum [25], where the measured signal is too weak for quantitative analysis. Closer to the resonance maximum, the dispersion depends on the shapes of the PEC's of the Auger initial and final states and can be similar to the observed constant kinetic-energy behavior. This is also the case for HCl, where the molecular background does not disperse noticeably within the HWHM of the resonance maximum [12].

Electron-energy spectra measured at the $2p_{3/2,1/2}\rightarrow\sigma^*$ resonances at two angles and the extracted anisotropy parameter β are shown in Fig. 4. Overall, our values of β are similar to the ones extracted from the work of Menzel *et al.* [16]. The β's of the photon lines at selected photon energies are shown as crosses (in the case of our work) and have strong positive values, as would be expected for direct photoionization, which has directional preference along the direction of the electric-field vector.

D. Auger decay of Rydberg resonances

The next photon-energy region explored (203–209 eV) is the core-to-Rydberg excitations ($2p\rightarrow nl$). This region of the 2D map is expanded in Fig. 5 and plotted with a binding-energy scale, where transitions to the same final ionic states are aligned vertically. The first resonance in this region is $2p_{3/2}\rightarrow 4s$ at 204.23-eV photon energy (see Fig. 2). It has a width of 102(2) meV and, in contrast to HCl, is well separated from the $2p_{1/2}\rightarrow\sigma^*$ resonance. The spectrum at this

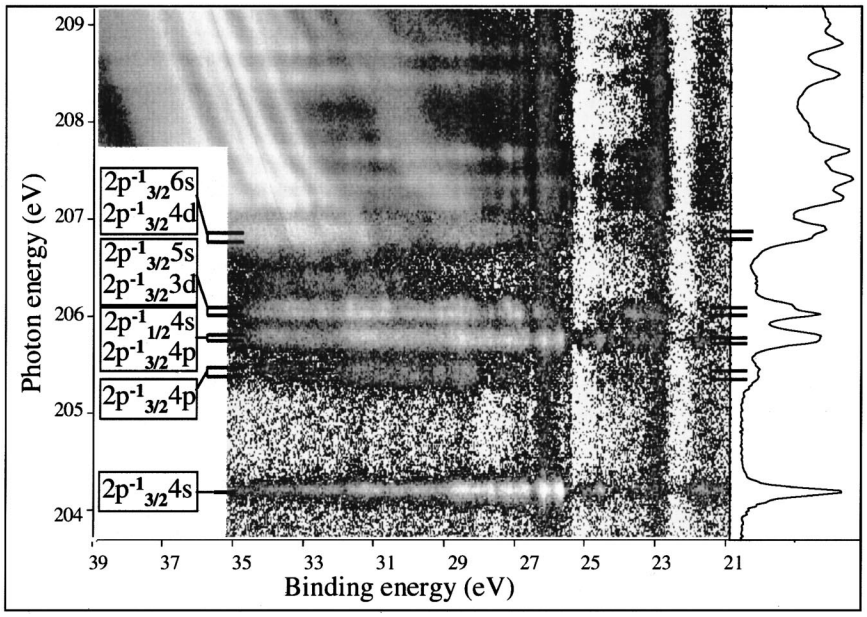

FIG. 5. 2D map of Auger electron emission at the Rydberg resonances measured at 54.7° relative to the polarization plane.

resonance is shown in the two lowest panels of Fig. 6 together with the extracted values of the anisotropy parameter. The binding energies of the resonant Auger lines 1–7 and their average β values are listed in Table I.

The angular distribution parameter β, shown in panel (d) of Fig. 6, has strong positive values for the photon lines and changes from -0.5 to 0.5 in the binding-energy region from 25 to 30 eV. There is no final ionic state assignment available yet.

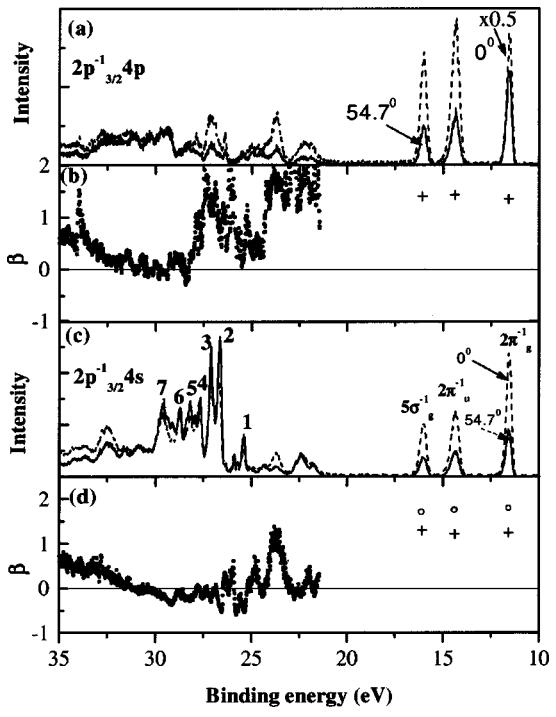

FIG. 6. Electron-energy spectra, measured at the $2p_{3/2}\rightarrow 4s$ and $2p_{3/2}\rightarrow 4p$ resonances. (a), (c) Electron-energy spectra of $2p_{3/2}\rightarrow 4s$ and $2p_{3/2}\rightarrow 4p$ resonances, taken at 0° and 54.7° relative to the polarization plane; (b), (d) the angular parameter β; open circles are the values from Ref. [16] and crosses are this work.

The next resonance, $2p_{3/2}\rightarrow 4p$, is centered at 205.44 eV in the summed electron yield. It is broader than the $2p_{3/2}\rightarrow 4s$ resonance, 281(40) meV, and weaker than the corresponding resonance in HCl. As was seen in HCl [12], the broadness of this resonance could be explained by assuming that it consists of two overlapping peaks corresponding to the molecular field splitting of the $2p_{3/2}$ core orbital into $2p_{3/2,1/2}2p_{3/2,3/2}$ components (using $nl_{j,m}$ notation). It is difficult to extract separate kinetic-energy spectra for each of the two components, but it is visually discernible that there are two overlapping resonances in this photon-energy area from the 2D map (Fig. 5). Electron spectra taken, separately from the data of Fig. 1, with good statistics at two angles on the resonance maximum of the $2p_{3/2}\rightarrow 4p$ (combining both components) and its β parameters are also shown in Fig. 6.

It is evident from the 2D map (Fig. 5) that the next higher Rydberg resonance structure in the photon-energy range between 205.7 and 206 eV consists of two peaks; one of them

TABLE I. Binding energies and angular distribution parameters β of peaks 1–6 in decay of the $2p_{3/2}\rightarrow 4s$ resonance [panel (c) of Fig. 6].

Peak number	Binding energy (eV) ±0.02	β ±0.1
1	25.42	−0.4
2	26.67	−0.4
3	27.11	−0.3
4	27.70	0
5	28.19	−0.3
6	28.74	−0.1

is $2p_{1/2} \rightarrow 4s$, and another is as yet unassigned at 205.8 eV. The width of the peak is 205 meV, twice the width of the $2p_{3/2} \rightarrow 4s$.

The Auger spectra intensities of higher Rydberg states gradually shift towards higher binding energies. This is probably due to the weakening of the influence of the spectator electron and higher shakeup probability [9]. Finally, resonant Auger lines smoothly merge into the normal Auger lines through a strong postcollision interaction (PCI). The energy shift of the normal Auger lines, caused by the PCI between the outgoing slow $2p$ photoelectron and the Auger electron, can be seen through threshold down to the Rydberg states. (The $2p$ ionization thresholds are marked in Fig. 1 from Ref. [17].) The shift below the threshold could be attributed to the screening effect of the bound, core-excited state. No marked difference can be observed between the energy shift of the Auger lines in the spectra taken at different angles. The normal Auger lines, marked as 4 in Fig. 1, at the $2p_{1/2}$ threshold ($h\nu = 209.42$ eV), is shifted by about 120 meV with respect to its position 1 eV above the threshold, in both 54.7° and 0° spectra.

IV. CONCLUSION

The 2D maps of electron emission from Cl_2 $2p$ ($L_{2,3}$) excitations were measured at two angles of electron emission. The 2D mapping technique makes it possible to study various characteristics over large kinetic-and photon-energy regions, since it allows one to follow the evolution of different decay channels and to recognize processes such as resonance enhancements that are difficult to notice in the single kinetic- or photon-energy spectrum.

In the case of Cl_2, we have found that photoelectron lines do not resonate at the Rydberg resonance energies, which means that the participator Auger decay channels are much weaker compared to the spectator Auger process, in contrast to the observations for HCl. The structure of the electron-emission spectrum at the $2p^{-1}\sigma^*$ resonances led to the conclusion that they decay dominantly via molecular Auger decay. The conclusion was further supported by the observed angular distribution of the Auger electrons. However, our measurements do not reveal energy shifts of the molecular Auger lines as a function of photon energy, which is, according to earlier works on HCl, one of the features distinguishing the molecular and atomic decay processes. In addition, the excitation and decay of the $2p \rightarrow nl$ Rydberg resonances were examined in high photon- and electron-energy resolution and a rich absorption fine structure was found, with different intensity distributions in their corresponding Auger decay spectra. Calculations of the Cl_2^+ Auger final ionic states are needed to interpret the observations in further detail.

ACKNOWLEDGMENTS

This work was supported by the Department of Energy, Office of Sciences, Basic Energy Sciences, Chemical Science Division. The ALS is operated by DOE, BES, Material Science Division. B.L. is indebted to the Alexander von Humboldt Foundation for partial financial support.

[1] U. Becker, R. Hölzel, H. G. Kerkhoff, B. Langer, D. Szostak, and R. Wehlitz, Phys. Rev. Lett. **56**, 1455 (1986).
[2] O. Hemmers, F. Heiser, J. Eiben, R. Wehlitz, and U. Becker, Phys. Rev. Lett. **71**, 987 (1993).
[3] U. Hergenhahn and U. Becker, J. Electron Spectrosc. Relat. Phenom. **72**, 243 (1995).
[4] U. Becker and A. Menzel, Nucl. Instrum. Methods Phys. Res. B **99**, 68 (1995).
[5] A. Kivimäki, M. Neeb, B. Kempgens, H. M. Köppe, and A. M. Bradshaw, Phys. Rev. A **54**, 2137 (1996).
[6] S. Sundin, S. J. Osborne, A. Ausmees, O. Björneholm, S. L. Sorensen, A. Kikas, and S. Svensson, Phys. Rev. A **56**, 480 (1997).
[7] H. Aksela, E. Kukk, S. Aksela, O.-P. Sairanen, A. Kivimäki, E. Nõmmiste, A. Ausmees, S. J. Osborne, and S. Svensson, J. Phys. B **28**, 4259 (1995).
[8] E. Kukk, J. D. Bozek, W. Tcheng, R. F. Fink, A. A. Wills, and N. Berrah, J. Chem. Phys. **111**, 9642 (1999).
[9] E. Kukk, J. D. Bozek, and N. Berrah, J. Phys. B Lett. **51**, 51 (2000).
[10] E. Kukk, J. D. Bozek, and N. Berrah, Phys. Rev. A **62**, 032708 (2000).
[11] M. Neeb, M. Biermann, and W. Eberhardt, J. Electron Spectrosc. Relat. Phenom. **69**, 239 (1994).
[12] E. Kukk, A. A. Wills, N. Berrah, B. Langer, J. D. Bozek, O. Nayadin, M. Alsherhi, A. Farhat, and D. Cubaynes, Phys. Rev. A **57**, R1485 (1998).
[13] P. Morin and I. Nenner, Phys. Rev. Lett. **56**, 1913 (1986).
[14] E. Kukk, H. Aksela, O.-P. Sairanen, S. Aksela, E. Nõmmiste, A. Ausmees, A. Kikas, S. J. Osborne, and S. Swensson, J. Chem. Phys. **104**, 4475 (1996).
[15] A. Menzel, B. Langer, J. Viefhaus, S. B. Whitfiled, and U. Becker, Chem. Phys. Lett. **258**, 265 (1996).
[16] A. Menzel, Ph.D. thesis, Techn. Univ. Berlin (1994).
[17] D. Shaw, G. C. King, and F. H. Read, J. Phys. B **13**, L723 (1980).
[18] N. Berrah, B. Langer, A. A. Wills, E. Kukk, J. D. Bozek, A. Farhat, and T. W. Gorczyca, J. Electron Spectrosc. Relat. Phenom. **101**, 1 (1999).
[19] A. A. Wills, D. Ubri, M. Ukai, F. Currell, B. J. Goodwin, T. Reddish, and J. Comer, J. Phys. B **26**, 2601 (1993).
[20] N. Berrah, B. Langer, J. D. Bozek, T. W. Gorczyca, O. Hemmers, D. W. Lindle, and O. Toader, J. Phys. B **29**, 1 (1996).
[21] C. D. Caldwell, M. O. Krause, R. D. Cowan, A. Menzel, S. B. Whitfield, S. Hallman, S. P. Frigo, and M. C. Severson, Phys. Rev. A **59**, R926 (1999).
[22] A. Farhat, A. A. Wills, B. Langer, and N. Berrah, Phys. Rev. A **59**, 320 (1999).
[23] K. Ueda, J. B. West, N. M. Kabanchik, Y. Sato, K. J. Ross, H. J. Beyer, H. Hamdy, and H. Kleinpoppen, Phys. Rev. A **54**, 490 (1996).
[24] M. Braunstein and V. McKoy, J. Chem. Phys. **92**, 4887 (1990).
[25] P. Salek, F. Gel'mukhanov, and H. Ågren, Phys. Rev. A **59**, 1147 (1999).